Interim Progress Report on NASA Grant NAG5-2232

"Receiver Design, Performance Analysis, and Evaluation for Space-Borne Laser Altimeters and Space-to-Space Laser Ranging Systems"

for the period of Oct. 16, 1995 to April 14, 1996

Frederic M. Davidson
Xiaoli Sun
Christopher T. Field

Department of Electrical And Computer Engineering
The Johns Hopkins University
Baltimore, MD 21218

May 1996

Design and Performance Measurements of the GLAS Breadboard Altimeter Receiver

Xiaoli Sun
Department of Electrical and Computer Engineering
The Johns Hopkins University
Baltimore, Maryland 21218

May 1996

Abstract

We report here the design and the performance measurements of the breadboard receiver of the Geoscience Laser Altimeter System (GLAS). The measured ranging accuracy was better than 2 cm and 10 cm for 5 ns and 30 ns wide received laser pulses under the expected received signal level, which agreed well with the theoretical analysis. The measured receiver sensitivity or the link margin was also consistent with the theory. The effects of the waveform digitizer sample rate and resolution were also measured.

1 Introduction

The mission of the Geoscience laser altimeter systems (GLAS) is to measure the surface topography of the earth, especially the ice sheets at the poles, using a space borne laser altimeter. The laser altimeter measures the time of flight of the laser pulses, and, consequently, determine the altitude of the target given the spacecraft orbit altitude. The laser altimeter can also measure the albedo and the average slope of the target area under the laser footprint through the received pulse energy and pulse width. The receiver has to first detected signal in the presence of the noise before measuring the above pulse parameters. GLAS will also have a cloud lidar channel using frequency doubled Nd:YAG laser and photon counting detectors. We are currently developing the breadboard lidar receiver and the results will be reported in a later time.

The laser transmitter of the GLAS laser altimeter consists of a diode pumped Nd:YAG laser at its fundamental wavelength, 1064 nm. The laser pulse width is 4 to 6 ns FWHM and the the transmitted pulse energy is specified to be 100 mJ. The most sensitive photodetector at this near infrared wavelength is the IR enhanced Si APD manufactured by EG&G. The Mars Observer Laser Altimeter (MOLA) [1] [2] used a similar laser transmitter and the same Si APD photodetector. MOLA used a simple pulse leading edge timing circuitry to measure the time of flight of the laser pulse. The GLAS laser altimeter will digitize the received waveform and calculate the pulse centroid arrival time, the pulse energy, and the rms pulse width.

The ranging accuracy of a space borne laser altimeter such as GLAS has been studied in theory by Gardner [3] [4]. The receiver probability of detection vs. false alarm for an APD based receiver has also been studied by us [5]. The link margin which we calculated for MOLA was consistent with the test data.

We have recently built a breadboard GLAS altimeter receiver along with a full

function laboratory test setup. We have achieved a ranging accuracy of better than 2 cm with 5 ns FWHM received laser pulses at the expected received signal level. We also achieved a rms ranging error of less than 10 cm for 30 ns FWHM received pulse, which corresponds to a 3 degree slope ground target area and is considered as the typical received signal. The measured link margin for 20 ns wide pulse was about 10 dB. The rest of this report gives the details of the breadboard receiver design, the test setup, and the measured performance.

2 Description of the Breadboard GLAS Altimeter Receiver

Figure 1. shows a block diagram of the GLAS breadboard receiver. The key components are described in the following subsections.

2.1 The Si APD, the Preamplifier, and the Post Amplifiers

The Si APD preamplifier module was custom made by EG&G Optoelectronics Canada. The Si APD chip itself was custom made by EG&G (RCA then) for McDonnell Douglas Astronautics Company per Document 77B27K003 (i.e. the specification) for the laser satellite communication project. The diameter of the APD active area was 700 μm. The quantum efficiency was 35-40% at 1064 μm wavelength, which was several times higher than those of ordinary Si APDs at this wavelength. Another feature of these APDs was the low hole to electron ionization coefficient ratio, $k_{eff} \approx 0.008$ as compared to $k_{eff} \approx 0.020$ for commercial devices. The lower value of k_{eff} led to lower excess noise from the APD electron multiplication process. These APDs also had a guard ring, a reverse biased PN junction, around the APD active area designed to reduce the surface leakage current due to space radiation damage. The break-down voltage of the APD was about 400 volts and the operating bias voltage was about 40 volts below the break-down point, which gave an average APD

gain of 100 to 150. The maximum gain was measured to be about 390 to 490. The commercial version of these APDs from EG&G are the C30954E [6], which has a higher value of k_{eff} and no guard ring.

The preamplifier used was a standard EG&G C30998-250 hybrid transimpedance amplifier [7]. The APD and the hybrid preamplifier circuit were custom integrated by the manufacture into a standard 14 pin DIP package [7, or EG&G catalog]. The feedback resistance of the preamplifier was $R_f = 5.6K\Omega$ and the equivalent input noise current spectral density was 2.6 $pA/Hz^{1/2}$ at 100 MHz and increased by about a factor of two (6dB) at 200 MHz. The electrical bandwidth of the preamplifier was 250 MHz. The APD electrical bandwidth was between 150 MHz and 250 MHz. The measured electrical bandwidth of the module was about 200 MHz. The measured pulse rise and fall times were about 2.5 ns. The linear dynamic range of the module was measured to be at least 23 dB in term of the input optical signal pulse amplitude (46 dB in electrical pulse amplitude). We did not used the preamplifier originally designed for McDonnell Douglas because their electrical bandwidth was narrower, 37 and 67 MHz, which might not support the 4 to 6 ns FWHM laser pulses of GLAS.

A 500 to 50 Ω buffer had to be used to drive 50Ω coax cable, since the preamplifier was designed to drive only 500Ω load. The buffer circuit was directly copied from the EG&G application note [8] with the exception that the AC coupling capacitor values were increased by a factor of 10 in order to minimize pulse undershoot. The buffer circuit was only necessary for the breadboard receiver at this development stage. Once we finalize the design of the detector assembly, the APD preamplifier module and the post amplifiers can be fitted into a small circuit card and no line driver and buffer is required.

The post amplifiers of the breadboard receiver consisted of a Hewlett Packard HP8447F amplifier which had two stages with the gains of 26 dB and 22 dB, respectively. The bandwidth was 0.1 to 1300 MHz. The maximum output power of

the second stage was rated 0.1 watts. A variable attenuator was put between the two stages to adjust the overall gain. A coaxial attenuator was also used before the HP8447F, as shown in Figure 1. We adjusted both the attenuators when we measured the receiver performance vs. input signal levels such that the average pulse amplitude was always roughly 600 mV. In the final design of the detector assembly, one of the post amplifiers will be a variable gain amplifier which can be programmed according to the input signal level.

2.2 The Receiver Time Base and the Time Interval Unit

The time of flight of the received laser pulses was determined by a counter/timer, a waveform digitizer, and a signal processing personal computer. The counter/timer provided the time base and measured the time from the transmitted laser pulse to the received pulse at the leading edge as it triggered the waveform digitizer. The waveform digitizer sampled the received waveform upon triggering. The computer calculated the pulse centroid time, the energy, and the width.

The counter/timer, which is often referred as the Time Interval Unit (TIU), was a Stanford Research Systems SRS620 universal time interval counter. Its 1.0 KHz reference output was divided by 100 to form the 10 Hz laser trigger signal. The frequency divider was made with ECL logics and it could divide the input by any integer from 1 to 255. We chose a 10 Hz laser firing rate for the ease of receiver signal processing.

The 10 Hz laser triggering pulse was also used as the TIU start pulse, because the timing jitter of the laser diode transmitter was sufficiently small in our test setup . In practice, the laser transmitter may have significant timing jitter with respect to the triggering pulses. A photodiode has to be used to pick-off the transmitted laser pulse to start the TIU.

The TIU was stopped by the trigger output of the digitizing oscilloscope which

was synchronized with each sweep. In case the oscilloscope missed the signal, a clear pulse could stop and re-arm the TIU. The clear pulse was generated by the Tennelec TC410A delay & gate generator and combined with the scope trigger output through a power splitter/combiner. The clear pulse came about 100 μs after the range gate was closed. Misses could easily be identified by looking at the arrival times of the detected pulses.

2.3 The Waveform Digitizer

The waveform digitizer consisted of a HP54720A digitizing oscilloscope with two HP54712A plug-ins, which provided 2 input channels at a maximum sample rate of 4 Gs/s each. The resolution of the A/D conversion was 8 bits. The sample rate could be changed to 2, 1, 0.5, 0.25, 0.1 Gs/s and etc. The acquired waveform contained a given length pretrigger data to include the entire pulse waveform regardless of the trigger point. The throughput of data acquisition and transfer over GPIB was rated greater than 50 waveforms per second.

The oscilloscope had a trigger output which was always synchronized with the beginning of each sweep when the input signal crossed the triggering level. As a result, the oscilloscope also served as a precision leading edge discriminator for the TIU. This greatly simplified the task of synchronization and alignment between the TIU and the waveform digitizer as compared to using separate discriminators.

The signal output from the post amplifiers was split between Channels 1 and 3 of the oscilloscope. The signal at Channel 1 was being digitized while the input at Channel 3 served as the triggering channel. A lowpass filter was inserted before Channel 1 to reduce the noise bandwidth while passing the signal with minimum distortion. The lowpass filter used was a TTE LT5-83M-50-2A five pole Bessel lowpass filter. The pulse width of filter impulse response was 4 ns FWHM, smaller than the pulse widths of the received signal which we tested. Bessel lowpass filters are known to

have maximum flat phase response which, consequently, gives minimum pulse shape distortion. We also experimented with different bandwidth Bessel lowpass filters but found little difference in the ranging accuracy.

Another lowpass filter was used in line with the triggering signal before Channel 3 to maintain a reasonably high detection probability while keeping the false alarm probability reasonably low. The 3 dB bandwidth of this filter was chosen according to the received laser pulse width.

To implement the range gate, the trigger mode of oscilloscope was set to "State Trigger" with Channel 3 as the trigger source and Trigger Channel 4 logic state as the precondition. The oscilloscope could only be triggered when the range gate signal at Trigger Channel 4 was high. The range gate was generated by another delay & gate generator, EG&G Ortec 416A, as shown in Figure 1.

The oscilloscope ran under its own internal clock, which was asynchronous with the TIU clock and the 10 Hz laser triggering signal. As a result, the time between the trigger point and the sampling times were always random. This was a desired property of this test setup because in reality the arrival times of the received pulses are unknown and must be assumed as random. The oscilloscope interpolated time between the triggering point to the first sampling time. The computer read this interpolated time and used that as the time origin when calculating the centroid of the pulse.

2.4 The Computer and the Data Processing Algorithms

Data acquisition and data processing were carried out by a 486DX 50MHz PC with a National Instrument AT-GPIB board. The PC obtained the waveform data from the oscilloscope and the TIU reading via the GPIB bus. We achieved a signal acquisition and processing speed up to 30 laser shots per second, which included reading the waveform, reading the counter/timer, converting the raw ASCII waveform data into

a numerical array, and calculating the pulse energy, centroid, and rms width. Note that the data acquisition and processing speed can be increased many times if the waveform digitizer and the TIU are directly connected to the high speed computer data bus.

The procedure of the data acquisition and processing was as follows: (1) Sending commands to initialize the oscilloscope and the counter/timer; (2) Reading and interpreting the preamble of the oscilloscope waveform, including the offset and step size of the vertical data of the waveform, the step size of the horizontal time axis; (3) Arming the oscilloscope and waiting for trigger; (4) Acquiring the waveform data and converting it to a numerical array; (5) Reading the time between the trigger point to the first sample point; (6) Reading the counter/timer; (7) Calculating the pulse energy, centroid, and rms width. Steps (3) through (7) were repeated 200 times to obtain a statistics of the measurements.

The waveform acquired for each received pulse was several times longer than the pulse duration, because it was impractical to determine a priori the proper amount of pretrigger data and the length of the waveform to be sampled. The segments of the waveform before and after the actual received pulse contained only background noise and could interfere with the signal processing. Therefore, the waveform data had to be truncated to include only the pulse itself before calculating the pulse parameters. The truncation algorithm consisted of moving along the pulse waveform in both directions from the triggering point until the vertical waveform data first fell below a preset truncation window threshold level. The choice of the threshold level affected the accuracy of the pulse parameter estimates and it was a trade-off between the error due to the background noise and the error from the signal truncation. We found a threshold of 5 to 10% of the peak pulse amplitude was appropriate.

The received pulse energy or the pulse area was calculated as

$$A = R_d \sum_{i=i_0}^{i_0+L} y_i \Delta t = R_d \Delta t \sum_{i=i_0}^{i_0+L} y_i \tag{1}$$

where R_d is the responsivity of the detector assembly in volts/watt, $y_i's$ are the waveform data from the oscilloscope, i is the index of the waveform data array, i_0 is the index at the beginning of the truncation, and L is the duration of the truncated signal. Note that we have used the summation to approximate the integral in the above equation. The waveform data from the oscilloscope was actually in the form $y_i = Y_i dy + y_0$ with Y_i's the integer valued A/D converter output and dy and y_0 the step size and the offset given in the preamble. The preamble data was acquired only once before the actual measurement started.

The pulse arrival time at the centroid was given by

$$\begin{aligned} T_c &= \frac{\sum_{i=i_0}^{i_0+L} t_i y_i \Delta t}{\sum_{i=i_0}^{i_0+L} y_i \Delta t} = \frac{\sum_{i=i_0}^{i_0+L} (tr_i + t_{0i} + i\Delta t) y_i}{\sum_{i=i_0}^{i_0+L} y_i} \\ &= tr_i + t_{0i} + \Delta t \frac{\sum_{i=i_0}^{i_0+L} i y_i}{\sum_{i=i_0}^{i_0+L} y_i} \end{aligned} \tag{2}$$

where $t_i = tr_i + t_{0i}$ is the sampling time, tr_i is the oscilloscope triggering time measured by the TIU, and t_{0i} is the time from the triggering point to the 0th sampling time. The value of t_{0i} was interpolated by the oscilloscope upon each triggering.

The target range was obtained by

$$r = \frac{cT_c}{2} \tag{3}$$

with c the speed of light.

The rms pulse width was computed using the following equation

$$\begin{aligned} \sigma_p^2 &= \frac{\sum_{i=i_0}^{i_0+L} (t_i - T_c)^2 y_i \Delta t}{\sum_{i=i_0}^{i_0+L} y_i \Delta t} = \frac{\sum_{i=i_0}^{i_0+L} \left(i\Delta t - \Delta t \frac{\sum_{i=i_0}^{i_0+L} i y_i}{\sum_{i=i_0}^{i_0+L} y_i} \right)^2 y_i}{\sum_{i=i_0}^{i_0+L} y_i} \\ &= \Delta t^2 \left[\frac{\sum_{i=i_0}^{i_0+L} i^2 y_i}{\sum_{i=i_0}^{i_0+L} y_i} - \left(\frac{\sum_{i=i_0}^{i_0+L} i y_i}{\sum_{i=i_0}^{i_0+L} y_i} \right)^2 \right] \end{aligned} \tag{4}$$

The signal acquisition and processing program was written using the LabVIEW Software by National Instrument. The computer also calculated the mean and the standard deviation of each measured parameters over a number of repeated measurements. In addition, we calculated the mean and the standard deviation of the TIU readings in order to test the receiver performance with leading edge timing as opposed to pulse centroid.

2.5 The High Voltage APD Bias Supply

The APD bias voltage was generated by an Analog Modules 521-5 programmable high voltage power supply. The output ripple was < 10 mV. The output voltage could be adjusted from 0 to 600 volts by varying the resistance of a trim potentiometer.

The value of the APD bias voltage was constantly monitored by a voltage meter and the current was monitored by an electrometer, as shown in Figure 1. The voltage drop across the electrometer was less than 1.5 mV according to the specification. As it turned out, the leakage current through the bypass capacitors on the high voltage line before the APD reached to about 100 nA, which sometimes was greater than the total photocurrent through the APD itself.

3 Test Setup and Optical Signal Calibration

3.1 Test Setup

The test setup for the GLAS breadboard altimeter receiver is shown in Figure 2. The test light source consisted of an InGaAs quantum well laser diode, EG&G C86125E, which emitted at about 1064 nm wavelength at room temperature. The laser diode could be continuously modulated to simulate the received optical signals from any type of target. The laser diode was mounted on a temperature controlled mount and the temperature was set to $20°C$. The DC bias current and the modulation signal were applied through a bias tee. The bias current was set to a few milliampere below

the lasing threshold. The measured output pulse rise and fall times were < 2 ns. Part of the signal laser beam was also split into a high speed PIN photodiode to monitor the actual laser output pulse shape.

The laser diode modulation signal was from a LeCroy LM410 400Ms/s arbitrary waveform generator which was programmed to generate Gaussian pulses of various widths. The timing accuracy of the output pulses with respected to the trigger was better than 0.5% the FWHM pulse width when using the TIU master clock as the external clock source.

The two delay generators before the arbitrary waveform generator were used to simulate the round trip propagation delay of the laser pulses. They were coax cable type and very stable and accurate, though the maximum delay was only 64 ns each. We will replace those two delay generators with an HP5359A high resolution time synchronizer, which is capable of generating up to 160 ms delay with less than $\pm 100\ ps$ timing jitter. The expected propagation delay for GLAS is 4.7 ms at a 710 km altitude orbit. Other digital delay generators, including the one inside the LM410 arbitrary waveform generator, had excessive amount of time jitter in the output waveform after delaying for more than 1 ms.

The signal laser beam went through a set of ND filters, one variable and a few fixed, to simulate the propagation loss of the optical signal. The laser beam then hit a corner cube which was mounted on a sliding rail, as shown in Figure 2. The reflected laser beam was directed to the APD through two beam splitters. The first one was used to combine the simulated background light with the signal and the second split part of the light into a monitoring optical power meter. The corner cube could be slid along the rail to test if the receiver responded to the actual target range variation. Both the APD and the optical power meter sensor were enclosed in a nearly light tight box. An interference optical bandpass filter with 10 nm FWHM bandwidth was used at the entrance of the box. The filter was angle tuned for the maximum

transmission of the signal light.

The background light was simulated with a light bulb driven by a stable DC power supply. The light was first coupled into a 200 μm diameter core optical fiber and then collimated with a lens at the other end of the fiber.

3.2 Receiver Optical Signal Calibration

The detector was first removed and replaced with a optical power meter sensor head to determine the ratio of the beam splitter which split the light between the APD and the monitoring optical power meter. The ratio had to be determined separately for the signal light which was polarized and the background light which was incoherent and unpolarized. The signal laser pulse repetition rate had to be increased to about 1 MHz in order for the optical power meter to have a reasonable reading. The focusing lens in front of the APD was a 10× microscope objective and the light spot size at the focal point should be well within 100 micron, which was much smaller than the 0.7 mm diameter APD active area. All the light after the focusing lens was received by the APD.

The APD and the power meter were then put back as before. The laser pulse repetition rate was set back to 10 Hz as in its normal operation mode. The output of the monitoring PIN photodiode was connected to the oscilloscope and the pulse area was measured by the integration of the waveform. The laser pulse repetition rate was increased to about 1 MHz to measure the pulse energy using the optical power meter while keeping the background light blocked. This was necessary because the power meter had a the minimum detectable power and a 0.1 s averaging time. Since the laser modulation signal was AC coupled, the effective bias current decreased at the high pulse repetition rate. We compensated for this bias current shift by raising it until the output laser pulse area was the same as that at 10 Hz. The laser pulse energy into the APD was given as the monitoring optical power meter reading divided by the

pulse repetition rate and multiplied by the beam splitter ratio. The laser pulse rate and the bias current were then restored to the original values after the pulse energy measurement.

The background light into the detector was obtained by multiplying the monitor optical power meter reading by the beam splitter ratio while blocking the signal laser. The level of the background light could be varied by changing the voltage of the DC power supply.

4 Measurement Results and Discussions

4.1 System noise floor and limits of the equipment

We first measured the system error due to the equipment used by feeding the 6 ns FWHM laser driving signal from the arbitrary waveform generator directly back to the receiver. The arbitrary waveform generator output was then reconnected to the the laser and the PIN photodiode output was connected to the receiver through a linear amplifier to test additional jitters due to the laser diode. The PIN photodiode was right at the laser output with a relatively strong input, the output was considered noiseless except for the jitter due to the laser.

Figure 3 shows the measurement results. Most of the range error at 4Gs/s, 0.4 cm or 25 ps, was from the time walk of the discriminator inside TIU. This was tested by bypassing the oscilloscope and directly feeding the signal into TIU. The dependence of the range error on the sampling rate was believed to come from the uncertainties in the time from the triggering to the first sampling point which was interpolated by the oscilloscope. The accuracy of the interpolation was 0.2 times the sampling interval according to the oscilloscope specification. Figure 3 also shows that the laser diode introduced very little additional jitter.

4.2 Effects of the quantization error of the waveform digitizer

The effects of the quantization error of the waveform digitizer was measured by changing the vertical scale of the oscilloscope with the arbitrary waveform generator output directly fed to the receive. The effective number of bits used by the waveform digitizer for the input signal was equal to the total number of bits divided by the fraction of the vertical span which the signal occupied. The rms ranging error was measured with the signal occupying 1/2, 1/4, 1/8, 1/16, and 1/32 full scale of the oscilloscope, which corresponded to 7, 6, 5, 4, and 3 bits out of the total 8 bit digitizer resolution. Since the input signal was a strong and almost noise free, the measured range error could all be attributed to the ADC quantization noise and the system noise floor.

Figure 4 shows the test results under 6 ns and 30 ns FWHM pulse width at 4Gs/s and 1Gs/s sample rate, respectively. It shows that we need at least 4 bits and desirably 5-6 bits A/D resolution in order to keep the quantization errors below 5 cm. The rms range error also increased as the sample rate became lower and the pulse width became wider, partly due to the sample rate effect and partly due to the increased error in the interpolation of the triggering to the first sample time. The accuracy of interpolated time became poorer as the slope of triggering signal decreased.

4.3 Receiver performance under 5 ns FWHM laser pulses and the effect of ADC sampling rate

The receiver performance was first tested with 5 ns FWHM laser pulses, which corresponded to shortest received pulse width as the GLAS laser pulse width was expected to be 4-6 ns FWHM. The effect of the waveform digitizer sample rate and resolution should be the most server under this condition because the number of samples per pulse was the fewest. The background light was turned off during this measurement. The total amount of detector post amplifier gain was adjusted according to the input

signal level so that the pulse amplitude always occupied about 50% of the full scale of the waveform digitizer through out the measurement.

The laser driving signal from arbitrary waveform generator had a Gaussian shape but the pulse width was limited to 6 ns. We had to set the laser bias current much lower than the threshold to obtain 5 ns FWHM pulses. Figure 5 shows the laser pulse shape.

Figure 6 shows the measured receiver rms range error as a function of the number of photons per pulse incident onto the Si APD at various sampling rate. The incident number of photons was obtained by

$$photons/pulse = \frac{E_r}{hf} \tag{5}$$

where E_r is the incident optical pulse energy in Joule and hf is the photon energy. The solid curve in Figure 6 was generated using the formula given by Gardner [3] [4] and including the system noise floor. The measurement results agreed well with the theory. The data in Figure 6 also shows that the sample rate should be 1Gs/s or somewhat higher, since the ranging error started to increase rapidly below 1Gs/s. We also found that slight change in the APD gain had little effect on the ranging error.

The expected received pulse energy for GLAS is 8,700 incident photons per pulse based on our GLAS link margin analysis assuming 0.2 target albedo. We have demonstrated that a ranging accuracy of better than 2 cm can be achieved at 1Gs/s sample rate when there is no pulse spreading, such as for flat target area.

Figures 7 and 8 shows the standard deviations of the measured pulse energy and pulse width normalized to the mean. The solid curves were again from the equations given by Gardner [3] [4]. The discrepancies between the measurement data and the theoretical analysis are still being studied.

4.4 Receiver performance for 30 ns FWHM received pulses

The receiver performance was then measured with 30 ns FWHM Gaussian shaped laser pulses, which corresponded to a 3 degree slope target under the 70 meter GLAS laser footprint. Figure 9 shows the laser pulse shape measured by the PIN photodiode at the laser and the amplified APD output waveform at the expected signal level.

Figure 10 shows the measured ranging error as a function of the number of photons per pulse incident to the detector at 1Gs/s and under zero and 5 nW background light. A lowpass filter with 20 ns FWHM impulse response was used before the oscilloscope trigger channel (lowpass filter #2 in Figure 1) in order to maintain a reasonable detection probability and a negligible false alarm rate at low input signal level. Note the use of the lowpass filter in the triggering channel mostly affects the receiver sensitivity under a given false alarm rate. It should have a very little effect on the receiver ranging accuracy once the signals were detected. The pulse centroid calculation process itself is a kind of lowpass filtering. We also tested the receiver ranging accuracy with different bandwidth lowpass filters and observed little change in the receiver performance.

The solid curve in Figure 10 was again generated from the theory by Gardner [3] [4] plus the system noise floor. The measurement results agreed well with theory except at very low input signal level. The reliability of the algorithm which truncated the signal pulse waveform out of the entire collected data became poor under low signal to noise ratio.

Figure 10 also showed that the background light we applied caused a very small degradation in the receiver performance at relatively high input signal level. The 5 nW background light was about what we expected for GLAS with the sun directly over head when using a 0.85 nm FWHM optical bandwidth filter at the receiver.

As mentioned earlier, the expected received pulse energy for GLAS is 8,700 photons per pulse. Therefore, we have demonstrated a ranging accuracy of 10 cm for 30

ns FWHM pulses at 1Gs/s sample rate under the expected input signal level.

5 Measurement of the Minimum Detectable Signal Level

The receiver link margin is given as the ratio of the expected received signal level to the minimum detectable signal level. The latter is often considered as the signal level under which the probability of the detection drops to below 90%. The minimum detectable signal level depends on the signal to noise ratio at the discriminator, which is not only a function of the pulse energy, but also a function of the pulse width, the background light, and the detector dark noise. The signal to noise ratio is optimized if the receiver noise filter matched the input signal. Because the received signal pulse shape is not known a priori, we have to use several noise filters each of which matches one type of input signal. The received signal which falls between the matched types will have a less than optimal probability of being detected.

We measured the probability of detection vs. incident optical signal level for 5, 10, 20, 60, and 180 ns FWHM received pulses through the matched filters, which were 5 pole Bessel lowpass filters of the same impulse response pulse width. Figure 11 shows the results of a measurement under a false alarm rate of 10^{-3}/20km ($10^{-3}/133\mu s$) and a background light level of 3-3.5 nW. The false alarm rate was determined by counting the number of triggers with the timer/counter while blocking the signal laser and leaving the range gate open all the time. The probability of correct detection was determined by counting the number triggers with the signal unblocked and a narrow range gate in alignment with the received signal pulses.

Figure 11 shows that the minimum detected signal levels were less than 900 photons per pulse for 5, 10, 20 ns wide pulses. Our calculated minimum detectable signal level for 20 ns wide pulse was about 830 photons per pulse, which was close to what we measured. A link margin of 10 dB was demonstrated for this case.

6 Future Works

The measurements of the ranging error will be repeated for other received laser pulse widths. The effects of the APD gain will be further investigated. The minimum detectable signal power at various pulse width will be repeated.

We will further study the theory developed by Gardner and enhance it by including more factors we encountered in our experiment, especially the photodetector characteristics on the ranging performance.

We will also develop a detector subassembly which includes the Si APD preamplifier module, a variable gain amplifier, and a power amplifier, all packaged in a well shielded metal housing. The receiver performance will then be tested again. The achievable receiver dynamic range with the variable gain control will be determined.

References

[1] M. T. Zuber, D. E. Smith, S. C. Solomon, D. O. Muhleman, J. W. Head, J. B. Garvin, J. B. Abshire, and J. L. Bufton, 'The mars observer laser Altimeter investigation.' *Journal of Geophysical Research*, Vol. 97, No. E5, pp. 7781-1197, May 1992.

[2] L. Ramos-Izquierdo, J. L Bufton, and P. Hayes, 'Optical systems design and integration of the mars observer laser altimeter,' *Applied Optics*, Vol. 33, No. 3, pp. 307-322, Jan. 1994.

[3] C. S. Gardner, 'Target signatures for laser altimeters: an analysis.' *Applied Optics*, Vol. 21, No. 3, pp. 448-453, Feb. 1982.

[4] C. S. Gardner, 'Ranging performance of satellite laser altimeters,' *IEEE Trans. Geoscience and Remote Sensing*, Vol. 30, No. 5, pp. 1061-1072, Sept. 1992.

[5] X. Sun. F. M. Davidson. L. Boutsikaris, and J. B. Abshire. 'Receiver characteristics of laser altimeters with avalanche photodiodes,' *IEEE Trans. Aerospace and Electronics Systems*, Vol. 28, No. 1, pp. 268-275, Jan. 1992.

[6] 'Large area long wavelength enhanced silicon avalanche photodiodes for general-purpose applications,' data sheet on photodiode C30954E. C30955E, C30956E, EG&G Optoelectronics Canada, Oct. 1988.

[7] Data sheet on silicon avalanche photodiodes, C30988 Series, EG&G Optoelectronics Canada, Jan. 1991.

[8] 'DC coupling and 50 Ω loading of transimpedance amplifiers,' Application Note, EG&G Optoelectronics Canada, Oct. 1993.

May 14, 1996

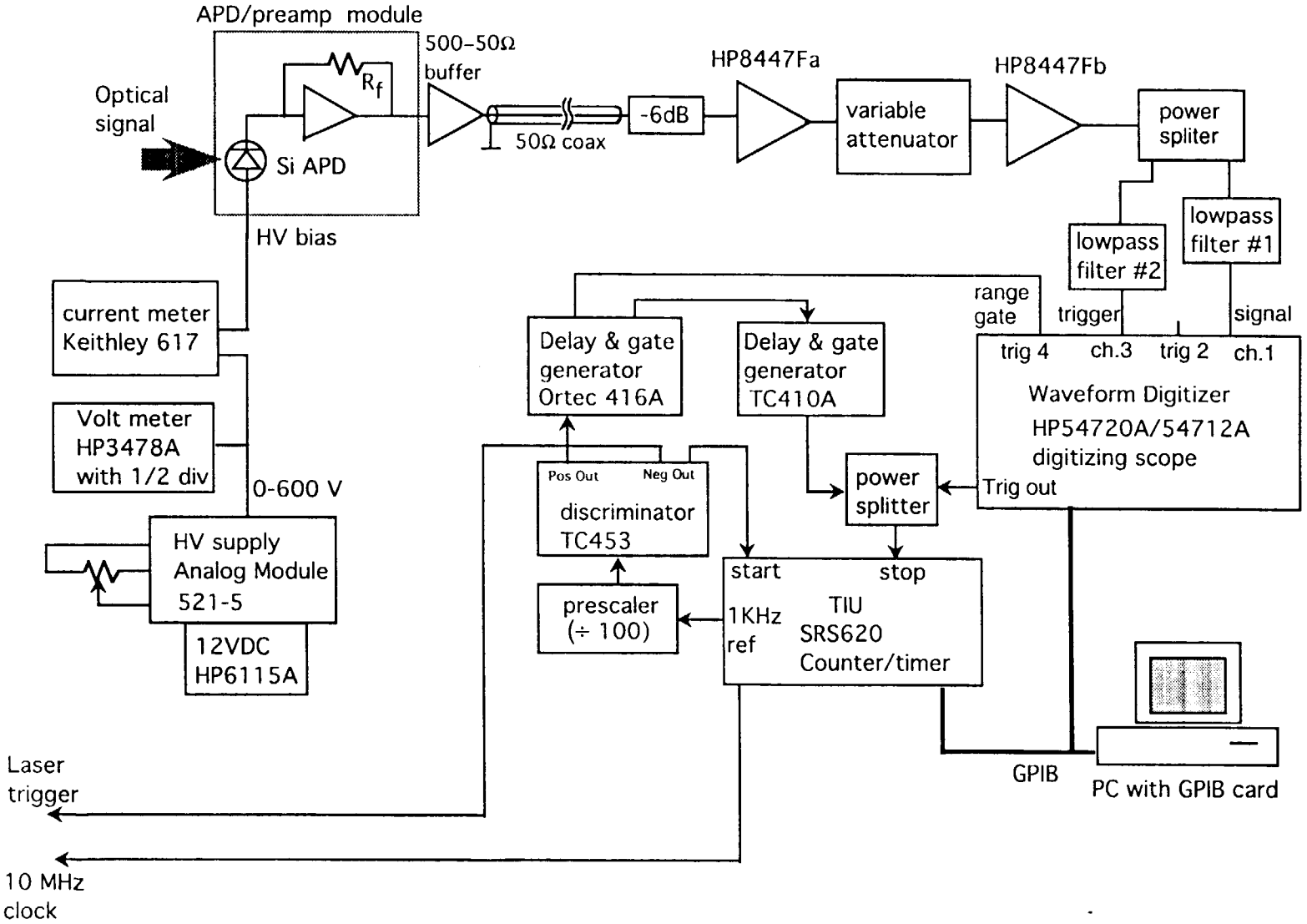

Figure 1. GLAS Altimeter Breadboard Receiver Block Diagram

May 14, 1996

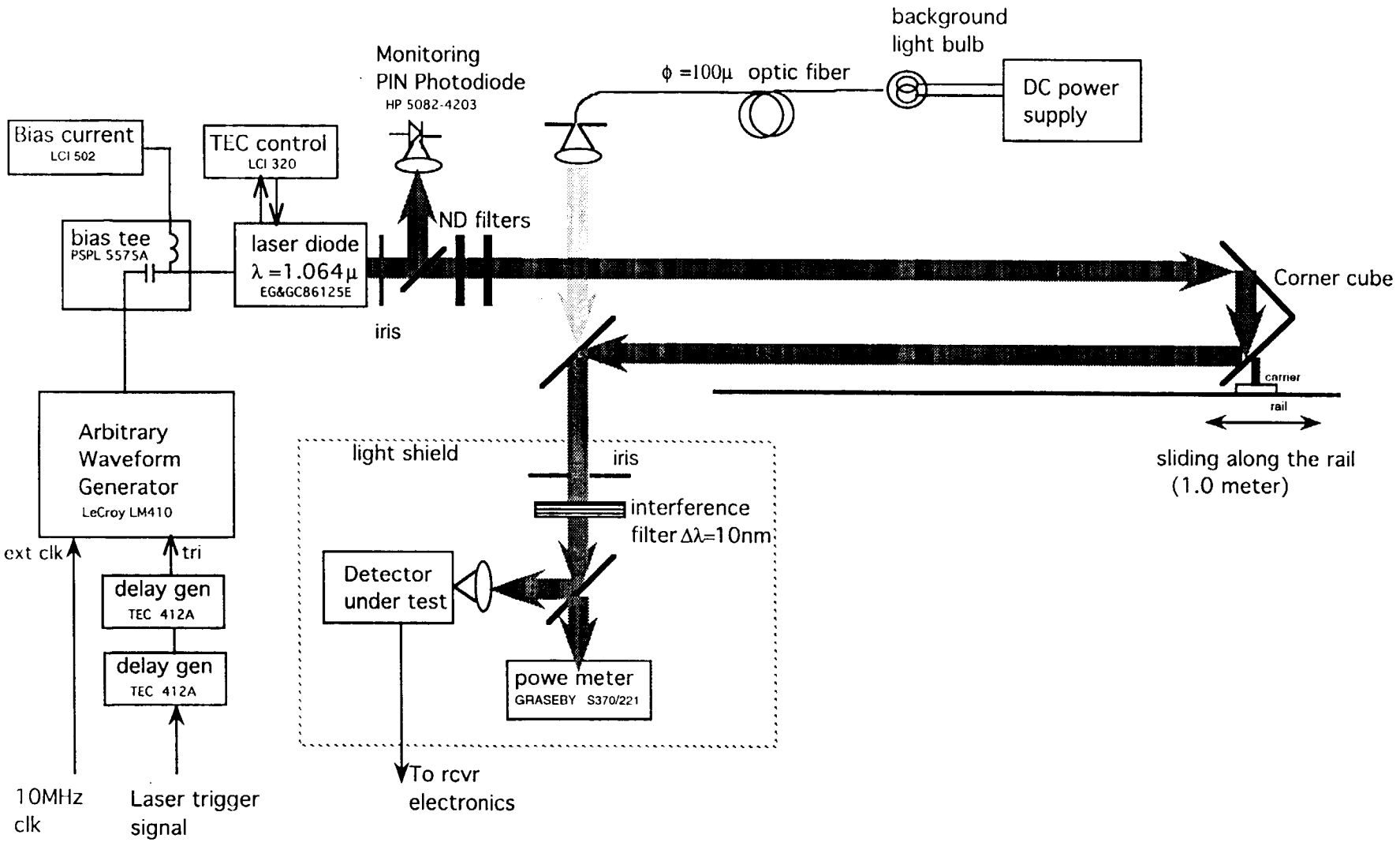

Figure 2. GLAS Altimeter Breadboard Receiver Test Setup

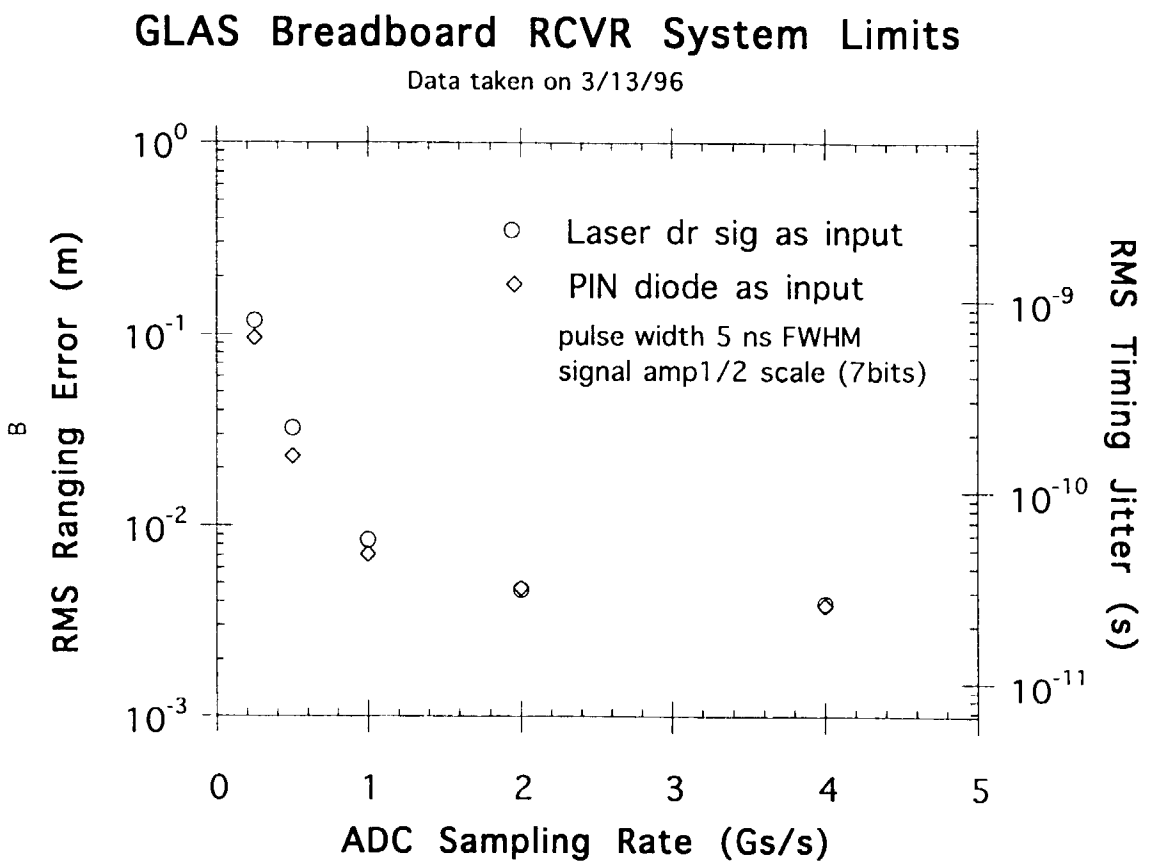

Figure 3. Measurement results of the system limits of the GLAS breadboard receiver and the test setup.

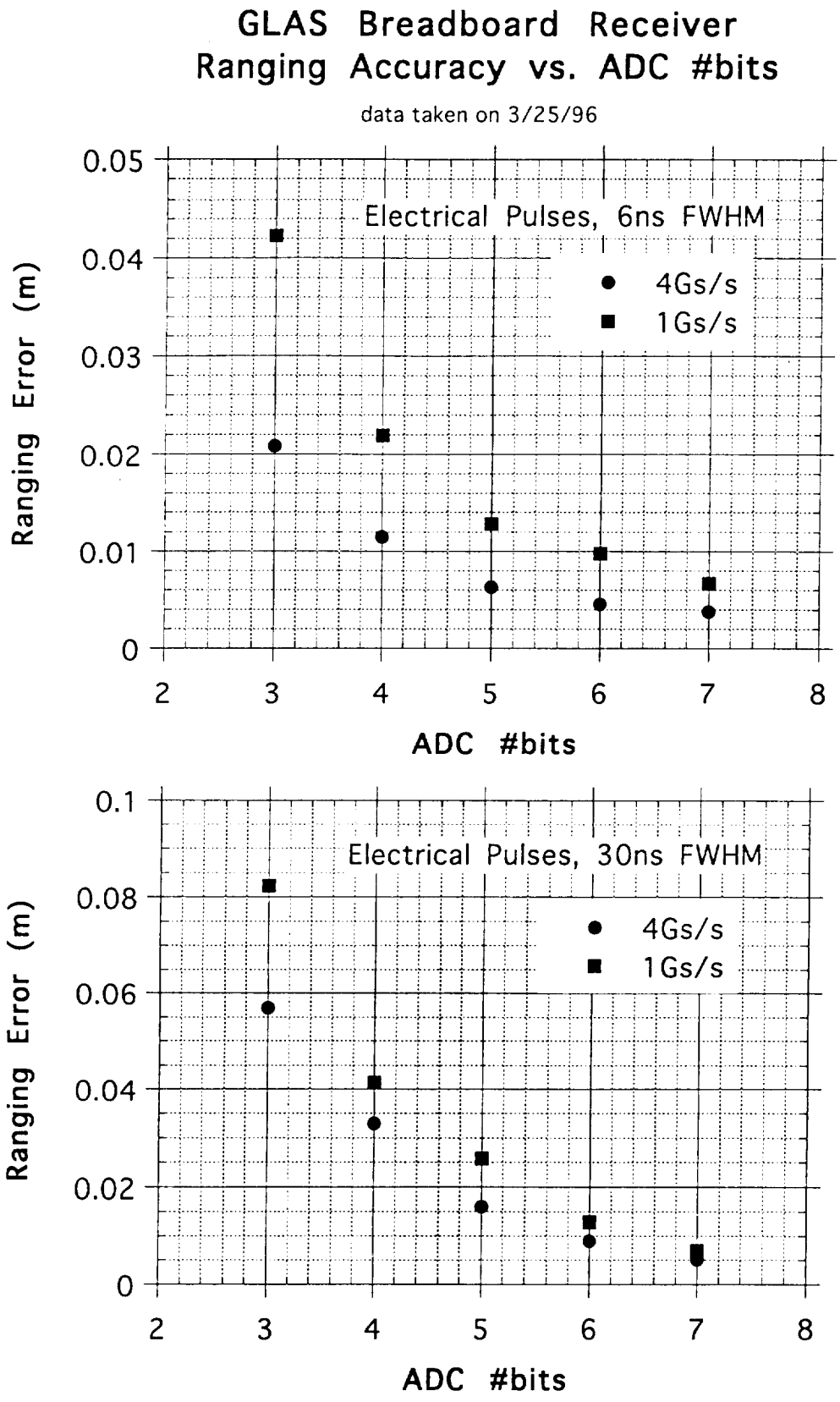

Figure 4. Ranging Error vs. ADC resolution (#bits).

Acquired: 02 FEB 1996 10:38:58.40 Printed

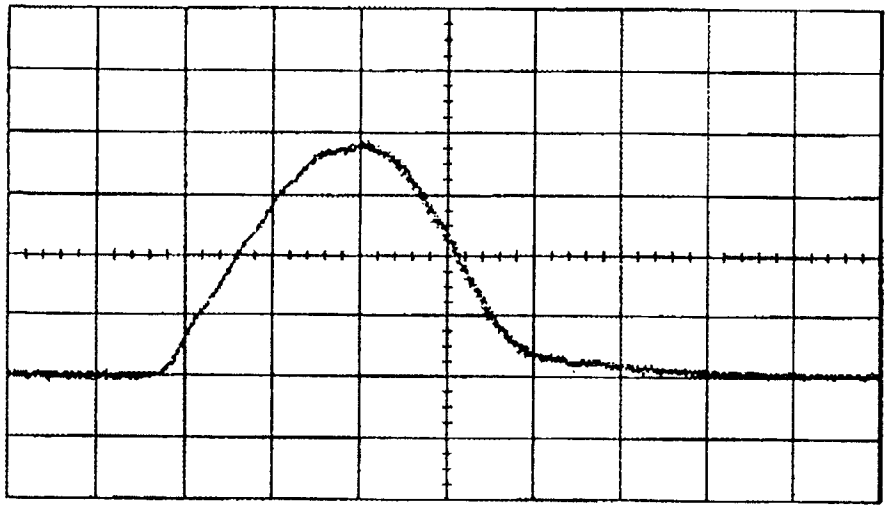

Channel 1 Scale 2 mV/div Offset 4.00 mV Input dc 50 Ohms
Time base Scale 2.00 ns/div Position 3.460 ns Reference center
Trigger Mode edge Source channel 1 Hysteresis normal Holdoff 60 ns
Level 4.8 mV Slope Pos
Measurement

	current
+ width(1)	5.0786 ns
V amptd(1)	7.680 mV

Figure 5. Laser pulse shape at 5 ns FWHM as measured by the PIN photodiode.

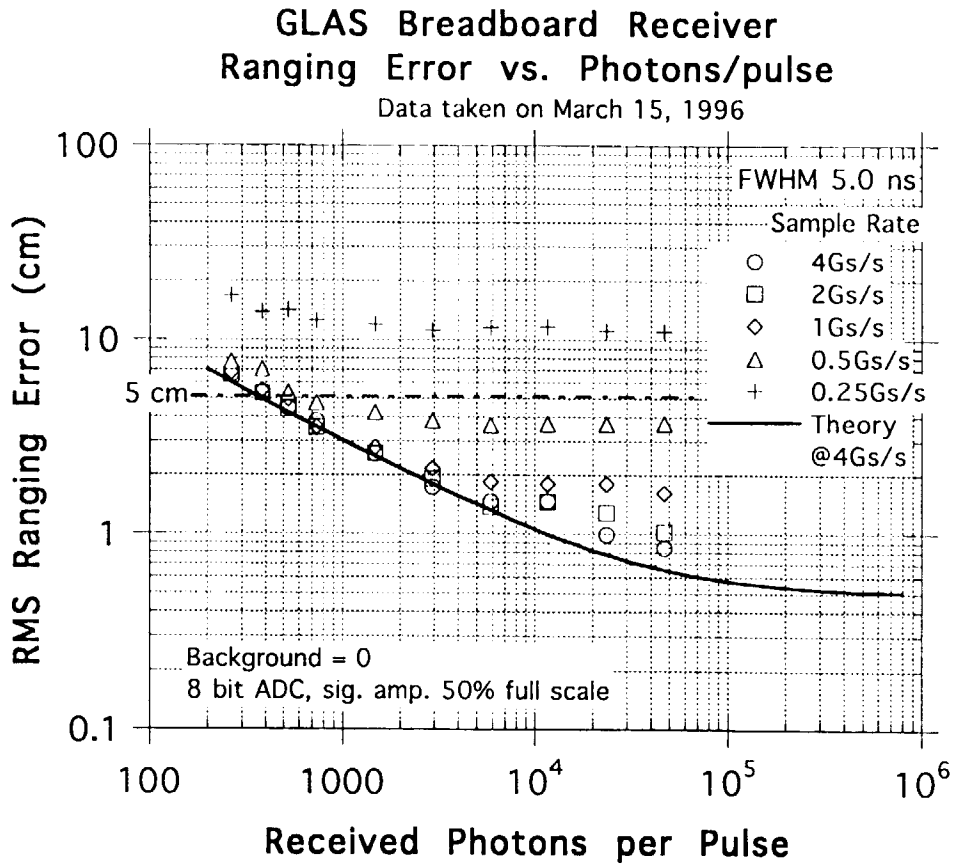

Figure 6. GLAS breadboard receiver ranging error as a function of the incident photons per pulse at various sampling rates for 5 ns FWHM received laser pulses.

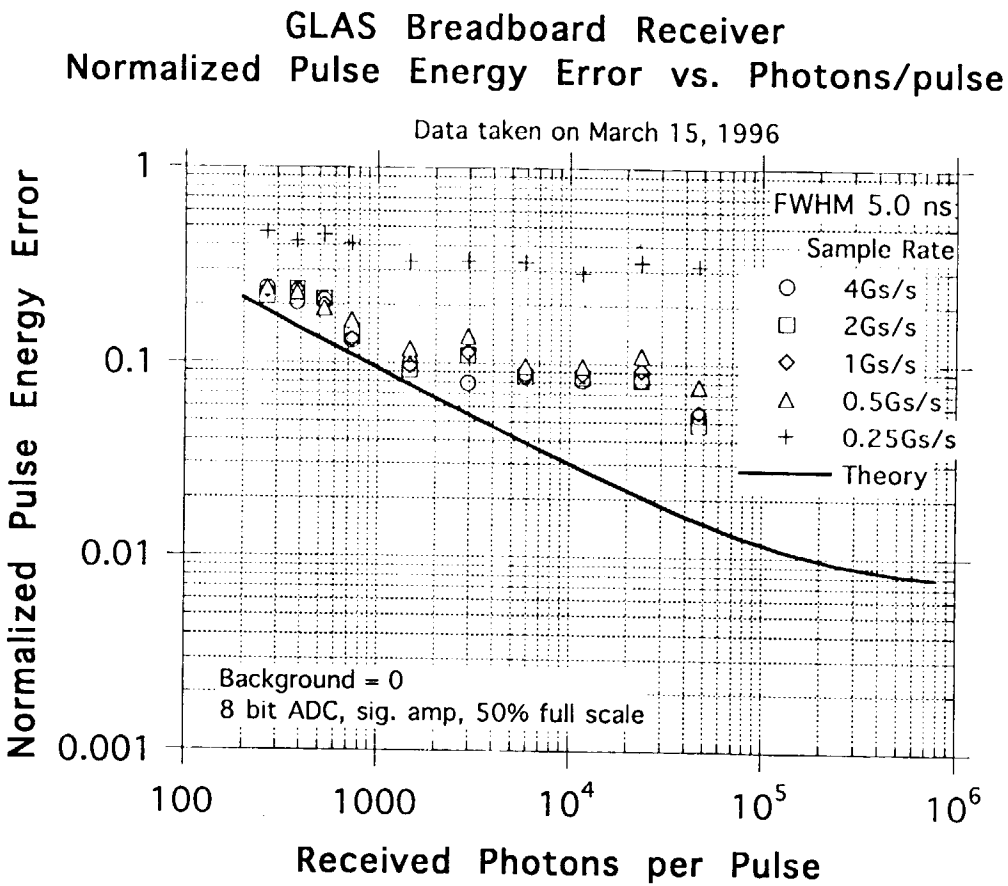

Figure 7. GLAS breadboard receiver pulse energy measurement error given as the standard deviation divided by the mean, vs. the incident photons per pulse at various sampling rates for 5 ns FWHM received laser pulses.

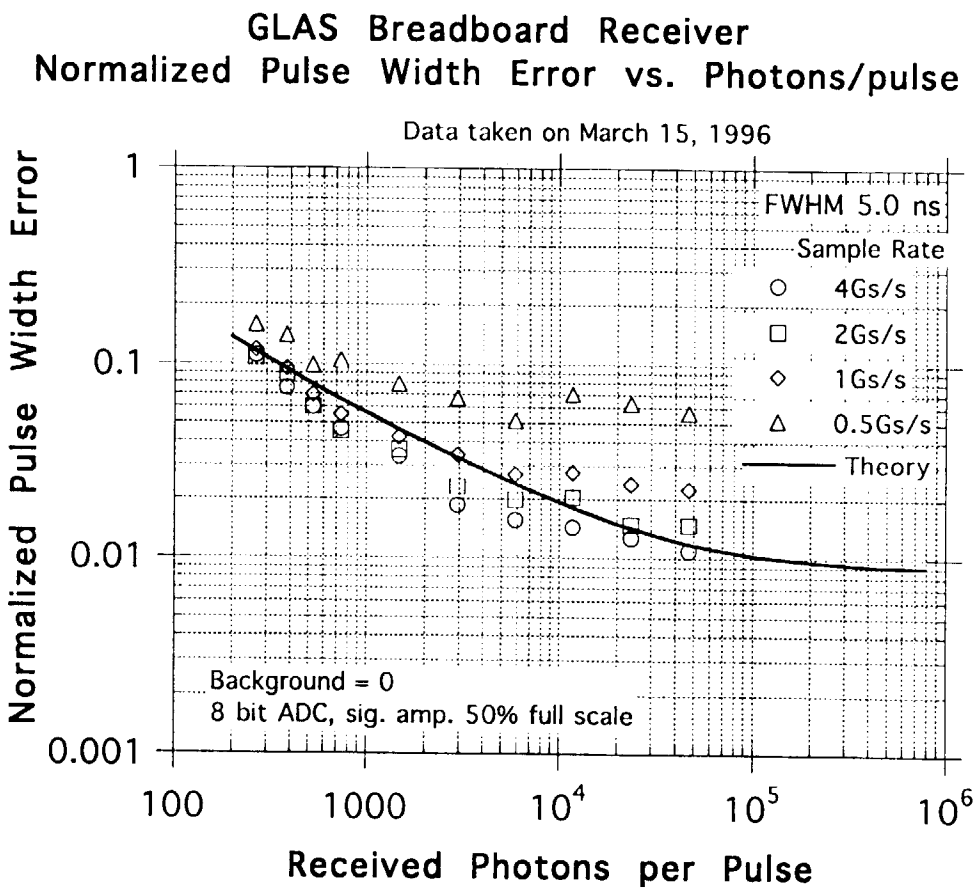

Figure 8. GLAS breadboard receiver pulse width measurement error given as the standard deviation divided by the mean, vs. the incident photons per pulse at various sampling rates for 5 ns FWHM received laser pulses.

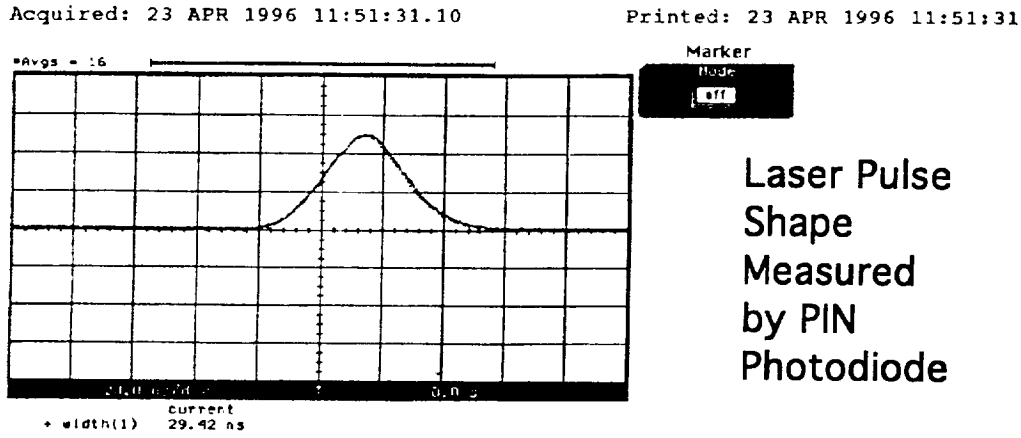

Laser Pulse Shape Measured by PIN Photodiode

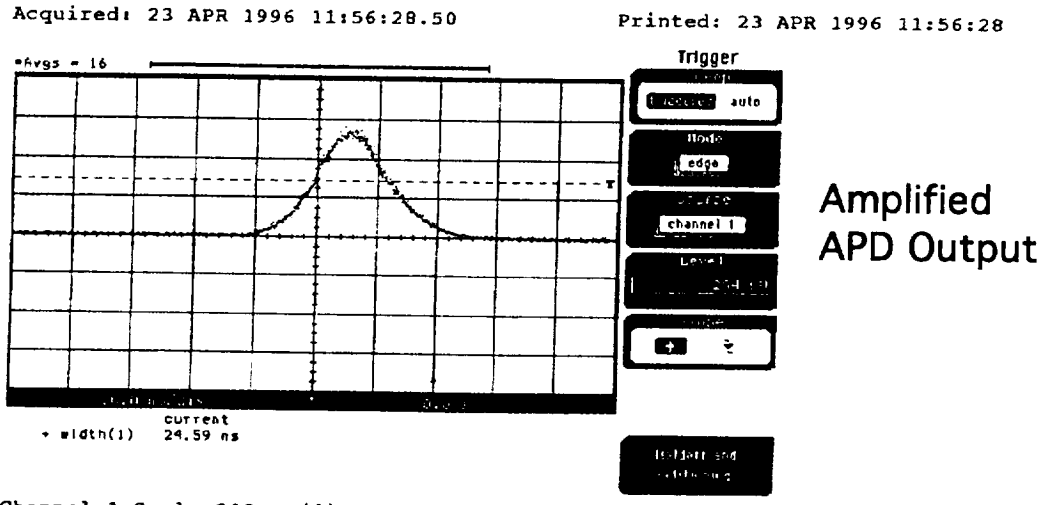

Amplified APD Output

Figure 9. Laser pulse shape at 30 ns FWHM measured by the PIN photodiode and the pulse shape output from the APD post amplifiers.

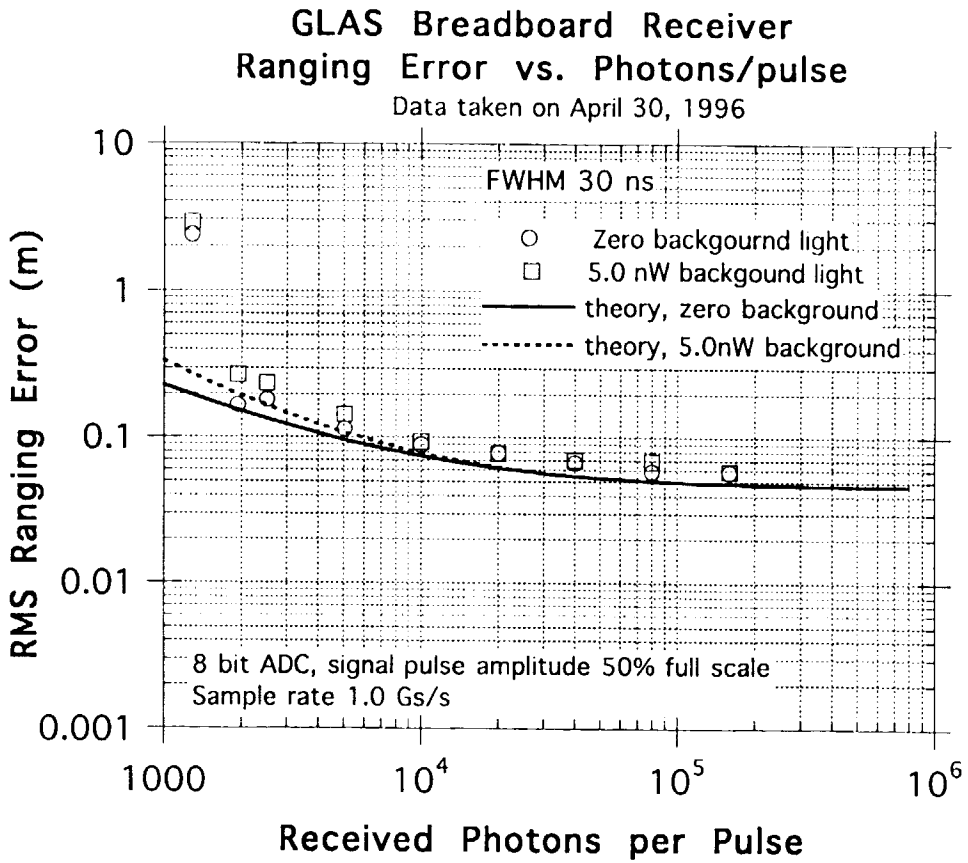

Figure 10. GLAS breadboard receiver ranging error as a function of the incident photons per pulse at various sampling rates for 30 ns FWHM received laser pulses.

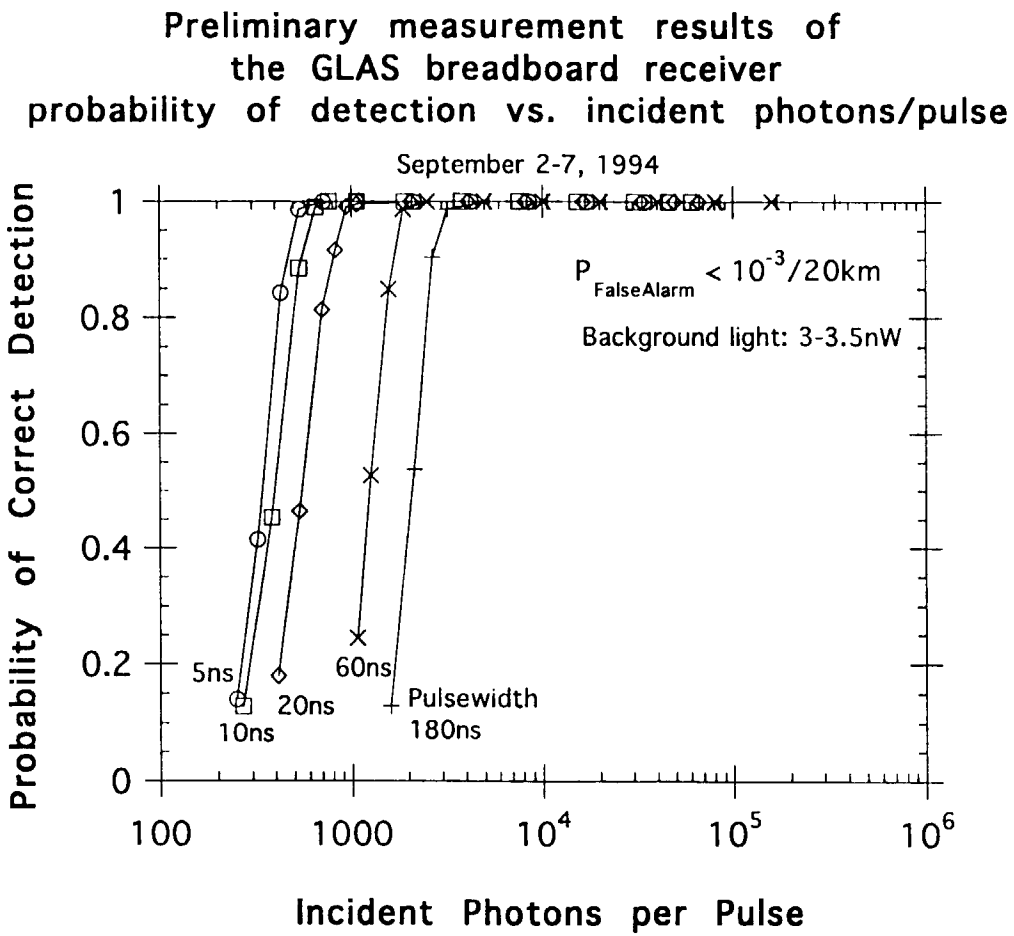

Figure 11. Preliminary measurement results of the GLAS breadboard receiver probability of detection vs. incident photons/pulse